Radar Cross-Section of Ceramic Corner Reflectors in the W-Band Fabricated With the LCM-Method

Kai-Daniel Jenkel, Benedikt Sievert, *Member, IEEE*, Andreas Rennings, *Member, IEEE*, Masoud Sakaki, Daniel Erni, *Senior Member, IEEE*, and Niels Benson, *Member, IEEE*

***Abstract*—Corner reflectors (CR), especially when combined with information coding, are potential candidates for radar beacon applications, which could be used for the self-localization of autonomous vehicles. In order to further improve the radar cross-section (RCS) of such devices, additively manufactured filled corner reflectors (FCR) made of ceramics in comparison to classical metal based CRs in the W-Band, were evaluated. The ceramic CRs were implemented using Lithography-based Ceramic Manufacturing (LCM), which is a novel high quality, high-resolution technology gaining traction in the RF community.**

***Index Terms*—Filled corner reflector, radar cross-section, RCS modification, 3D-printing, ceramic manufacturing, LCM-method.**

I. Introduction

CORNER reflectors (CR) are typical passive component candidates for localization or positioning scenarios in RADAR applications [1]. Examples are autonomous vehicles (e.g., rescue drones), possibly without line of sight or in a low visibility environment [2]. The most common materials for this application are metals with a known high radar cross-section (RCS) over a defined aperture angle. With respect to the self-localization of objects, however, the retroreflective properties of typical metal corner reflectors are limited by the aperture of the structure, so that the RCS drops sharply above 45° with regard to the perpendicular axis of its opening [3]. A potential way to bypass this limitation has been introduced by Buchberger et al. [4] using filled dielectric CRs. Their design, based on polymeric material, is a filled corner reflector (FCR), where the reflection occurs at the interface between the dielectric and air, using the transition from an optically denser to a thinner medium. This allows the electromagnetic wave to be coupled in through larger incidence angles. The group was able to demonstrate an improved RCS and Half Power Beam width (HPBW) with this concept, when compared to a classical metal CR. However, due to a high loss tangent and the relatively low permittivity of the applied polymers, the performance was limited [5].

To improve on this concept, low-loss materials with an enhanced permittivity are an approach, to increase the material permittivity anisotropy and thereby reduce losses at the FCR -air interface [6], [7]. A category of materials that meet these criteria are ceramics, which, as an added benefit also have high chemical and thermal resistance [8]. In recent years, ceramic materials have received increasing attention, especially for high-frequency technology, due to their dielectric properties [5] and the possibility for additive manufacturing, such as using the LCM (Lithography based Ceramic Manufacturing) method [9]. LCM is a multi-step process in which a green body is formed from a slurry by photopolymerization [10], followed by post-treatment which includes cleaning, drying, and a temperature process consisting of debinding and sintering to transform the printed green body into a dense ceramic component. This technique enables the rapid fabrication of complex ceramic geometries with excellent dielectric properties (e.g., low loss tangent [11]) and high resolution in the sub 200 μm range, making it particularly attractive for the field of radio frequency technology [12]. Current research examples using the additive manufacturing technology are ceramic resonator structures based on photonic crystals operating at 98 GHz with an unloaded Q of 2601 [13], [14], [15].

The aim of this research is to evaluate the performance of the FCR concept using 3D-printed ceramics with a high permittivity. Thus, 3D-printed alumina (Al_2O_3) with a relative permittivity of $\varepsilon_r = 9.5$ and loss tangent $\delta = 0.0004$ is used [14]. In extension to the previously published work in the framework of the IEEE RFID-TA 2022 conference [16], this work further evaluates the alumina FCR. A metallized open alumina CR is fabricated and used as a reference. Furthermore, the influence of the material is investigated and in addition to Al_2O_3, zirconia (ZrO_2) as an additional ceramic material system is analyzed. 3D-printed ZrO_2 has an even higher permittivity $\varepsilon_r = 27.6$ and a loss tangent of tan $\delta = 0.0025$ (according to manufacturer data obtained at 3GHz) [17].

The following contribution is divided into the design and simulation part of the FCR concept with CST Studio Suite, as well as the additive manufacturing part of the FCR and the measurement of its monostatic radar cross-section.

Manuscript received 31 January 2023; revised 8 March 2023; accepted 25 March 2023. Date of publication 10 April 2023; date of current version 19 July 2023. This work was supported in part by the German Federal Ministry of Education and Research (BMBF) as part of the KMU-innovativ Project: Elektronisches Sensorsystem zur sicheren Erkennung von Fußgängern und Radfahrern im autonomen Fahrzeugverkehr (SeeYou); in part by the German Research Foundation (DFG) through the CRC/TRR 196 MARIE (Project C09) under Project 287022738. *(Corresponding author: Niels Benson.)*

Kai-Daniel Jenkel, Masoud Sakaki, and Niels Benson are with the Institute of Technology for Nanostructures (NST), Faculty of Engineering, University of Duisburg-Essen, 47048 Duisburg, Germany (e-mail: kai-daniel.jenkel@uni-due.de; masoud.sakaki@uni-due.de; niels.benson@uni-due.de).

Benedikt Sievert, Andreas Rennings, and Daniel Erni are with the General and Theoretical Electrical Engineering (ATE), Faculty of Engineering, and the CENIDE—Center of Nanointegration, University of Duisburg-Essen, 47048 Duisburg, Germany (e-mail: benedikt.sievert@uni-due.de; andre.rennings@uni-due.de; daniel.erni@uni-due.de).

Digital Object Identifier 10.1109/JRFID.2023.3265079

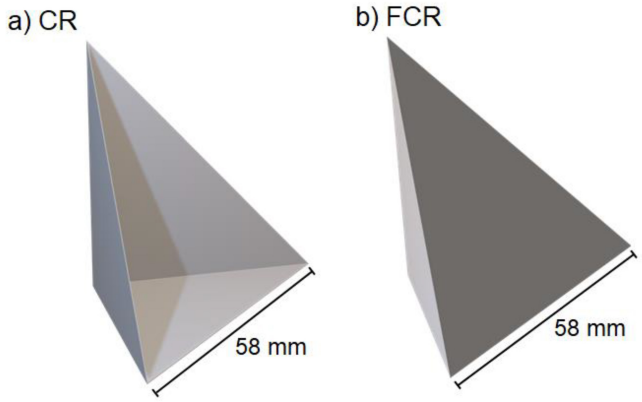

Fig. 1. Schematic design of an open corner reflector (a) and a filled corner reflector (b).

II. Materials and Methods

A. Design and Simulation

The design of the filled corner reflectors is based on the literature [4]. Thus, a FCR with an edge length of 58 mm is chosen to prove the validity of the concept and to evaluate the effect of alumina on the RCS. Fig. 1 a) illustrates the design of an open CR used as a reference in this work, and Fig. 1 b) illustrates the design for an FCR. CST Studio Suite was used to validate the FCR concept from a theoretical point of view. The Integral Equation Solver, based on the Multilevel Fast Multipole Method, was applied for this purpose.

B. Additive Ceramic Manufacturing

The fabrication of the FCR was done with the LCM-method, using a CeraFab 7500 from Lithoz GmbH. Aluminum oxide (Al_2O_3) and zirconium dioxide (ZrO_2) were processed using the commercial LithaLox HP 500 and Lithacon 3Y 230 slurry. The slurries contain ceramic particles with a volume fraction of 49 % (Al_2O_3) and 48% (ZrO_2) dispersed in a variety of proprietary polymers. The green body is printed layer-by-layer, with each layer being photopolymerized in accordance with the desired shape. The layer-height is chosen as 25 μm to ensure a high stability of the green body. The trigger for the polymerization is blue light (wavelength: 452 nm), which is transferred to the building platform in a 25 x 25 μm pixel pattern using a DLP (Digital Light Processing) projector. The light energy used for each layer is 200 mJ/cm^2 at an intensity of 60 mW, resulting in an illumination time of 3.3 s for alumina for each layer. For ZrO_2, an energy of 150 mJ/ cm^2 at an intensity of 140 mW was used, resulting in an exposure time of 1.1 s. After cleaning of the green bodies using an airbrush and Lithasol20/30 cleaning agents, a temperature treatment to burn out the polymer components and to densify the ceramic particles is used. This process is divided into three different steps. First a drying step up to 140 °C is applied, with low heating rates, to remove residues of the cleaning agents and volatile organic compounds. This step is essential for components with a high volume to avoid defects such as crack formation. Debinding happens in a second step, up to temperatures of 1100 °C to burn out the organic polymer network. In the third and final step the ceramic particles are sintered at temperatures of up to 1600 and 1450 °C for Al_2O_3 and ZrO_2, respectively, which also results into a sample densification and shrinkage. The complete temperature curves for Al_2O_3 and ZrO_2 are illustrated in Fig. 2.

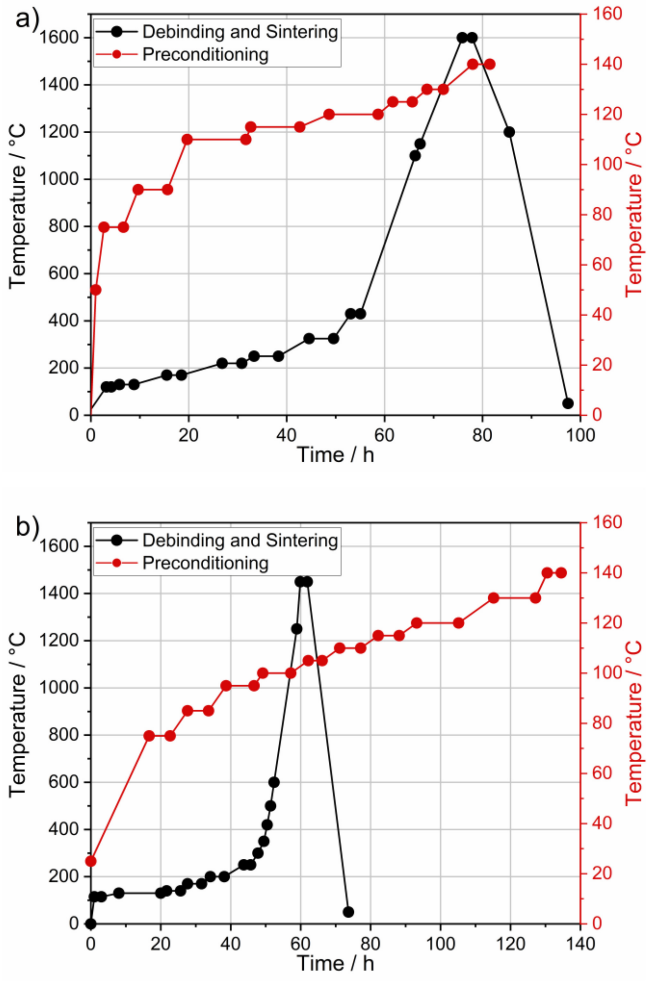

Fig. 2. Full temperature processes for Al_2O_3 (a) and ZrO_2 (b) (red line: Drying process, black line: Debinding and sintering).

C. Metallization of 3D-Printed Ceramics

For reference purposes, an open alumina corner reflector (as described in Section II-A) was fabricated and metallized using an electroless plating process. This process was adapted for the plating of ceramic components, as it was originally designed for polymer parts [18]. In this process, metal ions are locally reduced by catalytically activated reactions on the surface, so that the dielectric component is covered with a thin metal film. The metal used in this work is nickel. First, the ceramic components are cleaned in ethanol, isopropanol and deionized water for 5 min each in an ultrasonic bath. This step is necessary for a high surface quality. Afterward, the ceramic component is immersed in a palladium solution for 15 seconds. Subsequently, the component, now covered with Pd nuclei, is placed in a nickel solution consisting of: 50 g/L nickel acetate, 25 g/L sodium acetate and DEG monobutyl ether diluted as a stabilizer 1:1 diluted with distilled water. The

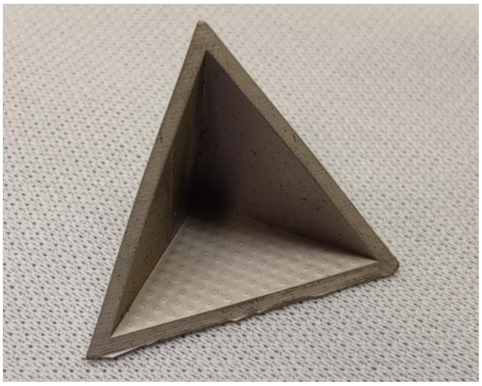

Fig. 3. Metallized CR consisting of Al_2O_3 produced by the LCM-method and plated with nickel (edge length: 22 mm).

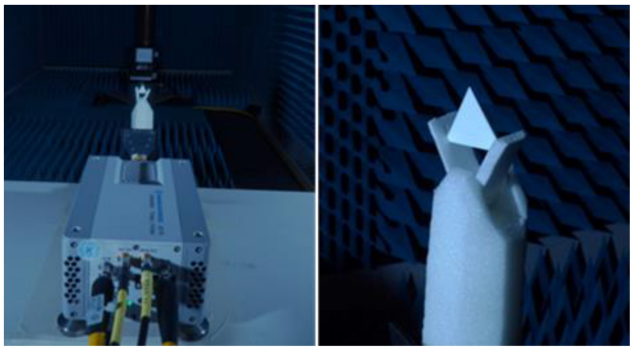

Fig. 4. Setup for the RCS measurement for the printed FCR.

temperature of 50 °C is maintained and 25 g/L of the reducing agent sodium hypophosphite is added. The reaction takes 30 min until a closed metal layer is deposited onto the component. Fig. 3 shows an open CR with nickel coating and same dimensions as the FCR, which is used as a metal reference for the measurement of the monostatic RCS.

D. RCS-Measurement

The RCS was investigated using a Rohde & Schwarz vector network analyzer (ZVA 40) in the 75-110 GHz frequency range as a function of the angle of incidence. The measurement took place in an anechoic chamber. Reference measurements, to ensure the proper functioning of the setup, were performed using two fixed diameter metal spheres. Time gating was applied to obtain a precise signal only from the reflector. A stepper motor was used to move the corner reflector in 1° steps. The setup is illustrated in Fig. 4.

III. Results and Discussion

As described in Section II-A, CST Studio Suite is used to simulate the RCS. The simulated monostatic RCS for a metal CR reference, a polymer FCR and an alumina FCR is illustrated in Fig. 5. All devices have an edge length of 58 mm [4]. For the metal CR, the characteristic side lobes are at incidence angles of $\Phi = 39°$, which represents the limit of the aperture. The half-power beam width (HPBW) is at about 38°, which is in good agreement with values reported in the literature [19].

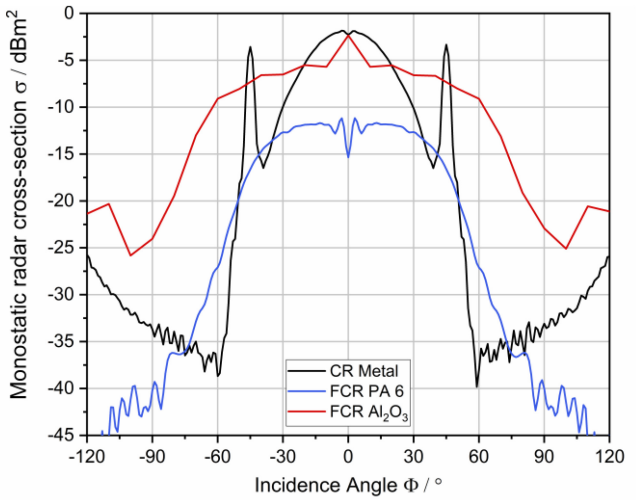

Fig. 5. Simulation results for the monostatic radar cross-section (RCS) as a function of the angle of incidence at 80 GHz. Black line: Metal corner reflector consisting of perfect conducting material as reference. Filled corner reflector (FCR) consisting of PA 6 (blue) and Al_2O_3 (red) (edge length: 58 mm).

This confirms the validity of the used simulation. Furthermore, Fig. 5 illustrates a FCR based on polyamide PA 6 ($\varepsilon_r = 3.06$ and $\tan\delta = 0.011$), which is typical for additive manufacturing purposes [20]. The simulation shows a change in the RCS for the polymer FCR when compared to the reference CR. In particular, the limitation of the opening angle is reduced, so that a broader aperture is observed. This results in an HPBW of 71° and thus an increase of 86% when compared to the metal CR. This confirms the findings from the literature that the FCR concept is a possibility to enhance the RCS [4]. However, the discussed disadvantage of the polymer is also evident, as the general RCS level has dropped significantly by up to 8 dBm^2 when compared to the metal CR. In contrast, the simulation for the alumina FCR shows an improved HPBW of 76°, which is an improvement of 100 % when compared to the metal CR, while the RCS level is comparable, due to the low loss of the material. Thus, alumina is a possible candidate material for a significant improvement of the RCS. Noticeable is a peak that can be observed at small angles of incidence. This is ascribed to a reflection at the first interface between air and alumina, which interferes constructively with the reflection at the rear interface of the FCR. The peak depends on the size of the FCR, as well as the frequency, and can be used to fine-tune the RCS. The interference effect is not considered for the parameter extraction of the HPBW.

For experimental validation of the simulation results, alumina FCRs were realized as described in Sections II-A and II-B. For this purpose, the size was limited to a FCR edge length of 22 mm, as otherwise crack formation is possible in the area marked as critical in Fig. 6 a) during temperature processing as outlined in the experimental section. The FCR after temperature processing is illustrated in Fig. 6 b), demonstrating the shrinkage taking place during this process.

The RCS measurement of these devices was performed as described in Section II-D, with the result being illustrated in Fig. 7. The comparison of the RCS at 80 GHz between the

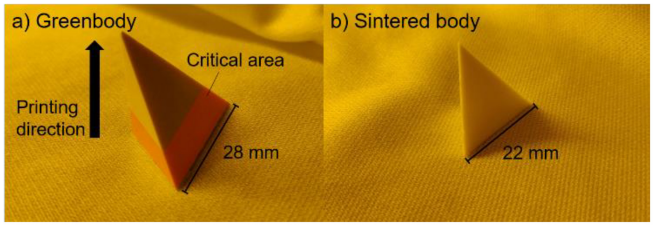

Fig. 6. Successfully printed (a) and sintered (b) FCR with a final edge length of 22 mm consisting of Al_2O_3.

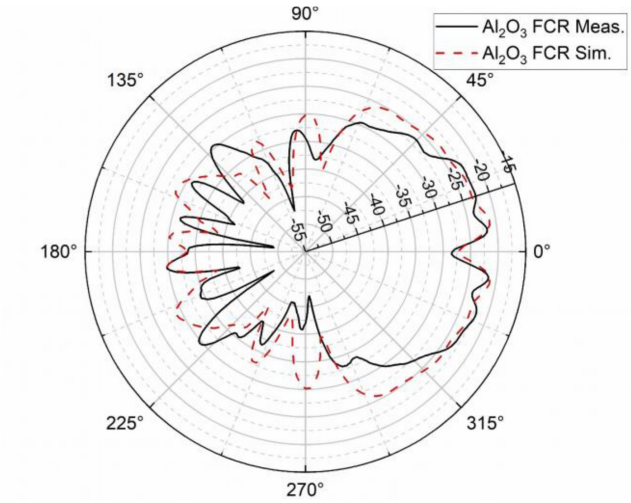

Fig. 7. Comparison of RCS-measurement (black) and simulation (red) for an alumina FCR (edge length: 22 mm) at a frequency of 80 GHz (RCS in dBm^2).

real and the simulated device shows good agreement. At small angles, there is a very good correlation between measurement and simulation, and the discussed interference effect is present in both cases. At larger angles, the RCS of the simulation is slightly higher when compared to the measurement. This can be seen, for example, in the HPBW, which is 64° for the measured FCR and 75.4° for the simulation. One reason could be the remaining of some porosity inside the material during sintering which causes internal reflections.

To compare this result to a classical CR, a reflector was realized as described in Section II-B using metallized alumina. This assures that size and anisotropic shrinkage are the same for all components. Fig. 8 compares the simulated and measured monostatic RCS of the metal CR. There is good agreement between simulation and measurement. The only significant deviations are in the side lobes at about ± 39°, which are less pronounced in the measurement. The HPBW of the simulation is 37°, while a value of 34° is observed in the measurement. Furthermore, Fig. 8 also compares the Al_2O_3 FCR measurement with the mentioned CR simulation and measurement. For the alumina FCR similar RCS for 0° and slightly lower RCS level for smaller angles can be observed, when compared to the metal reference. For angles larger than ±30° the advantage of the FCR concept is evident and higher RCS values are obtained. Furthermore, the limitation of the CR regarding the opening angle is apparent as already discussed above, which results in an 88 % increase in HPBW regarding the measurement while maintaining a similar RCS level.

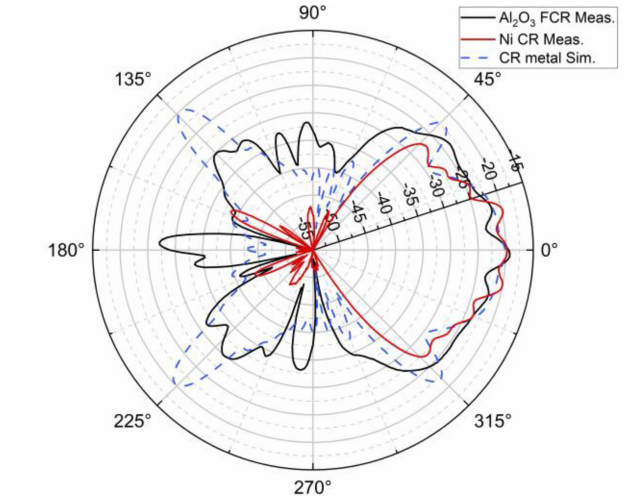

Fig. 8. Comparison of RCS-measurement of Al_2O_3 FCR (black) and metallized CR (red) at 78.5 GHz as well as a simulation of a metal CR with perfect conducting material (blue) (edge length: 22 mm) (RCS in dBm^2).

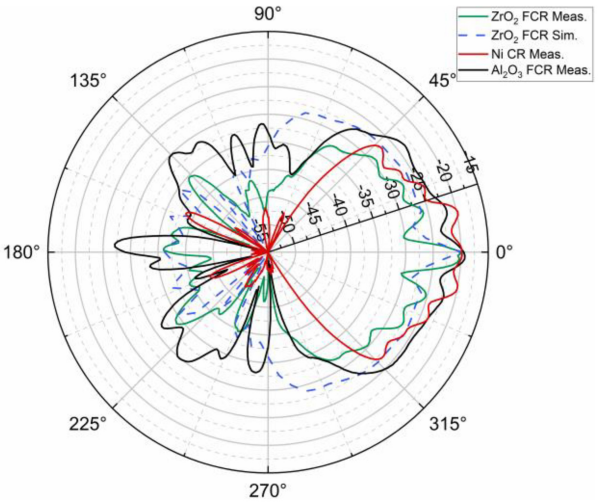

Fig. 9. Comparison of RCS-measurement at 78.5 GHz (green) for a FCR consisting of ZrO_2 and simulation (blue dashed). Measurement results for metallized CR (red) and alumina FCR (black) from Fig. 8 as reference (edge length: 22 mm) (RCS in dBm^2).

Thus, using the FCR concept in combination with low-loss ceramics, such as alumina, is a good possibility for corner reflector radar cross-section enhancement.

An additional benefit of using ceramics for this type of device, is that a wide range of materials with a large variation in refractive indices and otherwise low-loss properties are available [21]. In consequence, one approach to further improve the RCS by enhanced internal reflections could be an increase in the permittivity and thus the anisotropy in the refractive index. For this purpose, 3D-printed zirconia was used in this contribution, with a significantly higher permittivity ($\varepsilon_r = 27.6$) than alumina, yet on the down side with an increased loss tangent ($\tan\delta = 0.0025$) [17]. The zirconia FCR implementation is described in the experimental Section II-B. Fig. 9 illustrates the measured and simulated monostatic RCS spectrum of the realized zirconia FCR compared to the previous results for the alumina FCR and the metal reference. The alignment between measurement and

simulation agrees well for small angles. For larger angles, however, the simulation clearly overestimates the zirconia FCR RCS value. The HPBW gives a value of 150° for the simulation, which would be a great improvement. The measurement, however, only gives an HPBW of 62°. Still, for large angles over ± 45° a higher RCS for the ZrO_2 FCR in comparison to the metal reference is observed. Further, the HPBW of 62° indicates an improvement of 82 %, when compared to the metal reference. The observed large difference between measurement and simulation is most likely due to incorrect assumptions regarding the quality of the material and its dielectric properties. Especially for zirconia, the dielectric material properties are very dependent on the crystal structure of the solid. Meaning the permittivity can vary from 17 to almost 40, depending on which crystal phase (Monoclinic, Tetragonal or Cubic) or which ratio of the different crystal phases exist in the final sintered solid [22], [23]. The dielectric properties used for the simulation were determined on different samples by the material supplier for a frequency of 3 GHz and a sample density of 99.4% [17]. This is a limitation for our zirconia simulation, not just due to the unknown crystal phase composition of our part, but also because our experimental frequency range is the W-band, and therefore, the frequency dependence of the permittivity may further degrade the assumed permittivity value. In addition, the density of our samples was determined to be 97% using Archimedes principle measurements, which is most likely the consequence of a residual porosity, small cracks or defects, which may occur during the sample temperature treatment. This may lead to a further reduction of the effective permittivity. Therefore, in order to improve the accuracy of our zirconia RCS simulation, the permittivity of our specific material needs to be determined, for example using transmission measurements. Further, in order to improve the material of our zirconia FCR investigations on the material quality, such as using X-Ray Diffraction (XRD), and an optimized processing are required.

While the aim of the enhanced zirconia refractive index is to improve the FCR RCS by improved internal reflections at the ceramic-air interface, the concept also has a disadvantage, which is the coupling of the radiation into the FCR. Illustrated in Fig. 10 is the measured zirconia and alumina FCR RCS for an angle of incidence of 0° over a frequency range of 77-81 GHz. The signal level for both FCRs are periodically reduced from an approximate -20 dBm^2 level by destructive interference between incoming and reflected wave. However, this is much more pronounced for the ZrO_2 case and can reach up to a 25 dBm^2 in signal difference. Following Fresnel's equations for 0° incidence, the reflected power is enhanced when the difference between the refractive indices of the materials is higher, which might offer an explanation for this observation [24]. As this effect can be specifically adjusted, it may have the potential for coding applications.

IV. Conclusion and Outlook

Using the filled corner reflector (FCR) concept in conjunction with additive ceramic manufacturing of the materials alumina and zirconia, the HPBW of the RCS could be improved by more than 80% when compared to a standard metallized corner reflector reference. For alumina, the general RCS level was comparable to the metal corner reflector, making it an excellent alternative with a significantly wider aperture angle and HPBW (64°). While, for zirconia, material quality related issues have limited the significance of the RCS measurements, a pronounced interference effect for the 0° angle of incidence is observed. As an outlook, this effect, as well as the digital freedom that arises with using additive manufacturing, may have the potential for coding purposes in angular dependent localization problems. For this purpose, one can think of the integration of photonic crystal structures, such as using Bragg-reflectors.

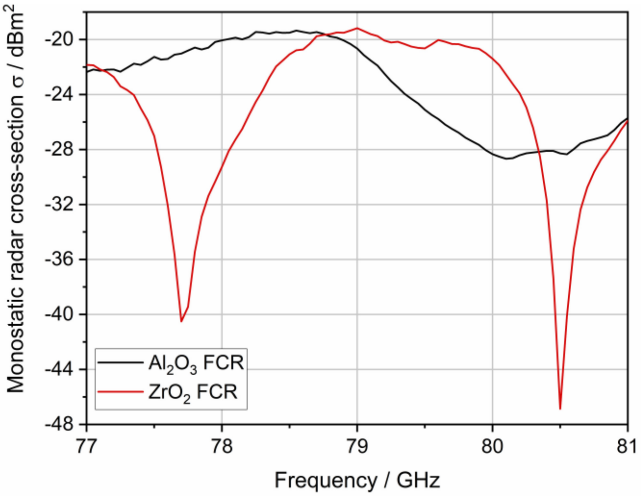

Fig. 10. Measured RCS for 0° incidence angle for Al_2O_3 FCR (black) and ZrO_2 FCR (red).

Acknowledgment

The authors would like to thank Martin Dehnen for his help with the ceramic metallization.

References

[1] B. R. Mahafza, S. C. Winton, and A. Z. Elsherbeni, *Handbook of Radar Signal Analysis*. London, U.K.: CRC Press, 2022.
[2] W.-J. Liao, Y.-C. Hou, C.-C. Tsai, T.-H. Hsieh, and H.-J. Hsieh, "Radar cross section enhancing structures for automotive radars," *Antennas Wireless Propag. Lett.*, vol. 17, no. 3, pp. 418–421, Mar. 2018, doi: 10.1109/LAWP.2018.2793307.
[3] G. Helmi, K. Ali, P. Philippe, and L. P. Oussmane, "Experimental results and numerical simulation of the target RCS using Gaussian beam summation method," *Adv. Sci. Technol. Eng. Syst. J.*, vol. 3, no. 3, pp. 1–6, 2018, doi: 10.25046/aj030301.
[4] C. Buchberger, F. Pfeiffer, and E. Biebl, "Dielectric corner reflectors for mmWave applications," *Adv. Radio Sci.*, vol. 17, pp. 197–203, Sep. 2019, doi: 10.5194/ars-17-197-2019.
[5] E. S. Rosker, R. Sandhu, J. Hester, M. S. Goorsky, and J. Tice, "Printable materials for the realization of high performance RF components: Challenges and opportunities," *Int. J. Antennas Propag.*, vol. 2018, pp. 1–19, 2018, doi: 10.1155/2018/9359528.
[6] F. A. Jenkins and H. E. White, *Fundamentals of Optics*, 4th ed. Chennai, India: McGraw-Hill, 1976.
[7] E. Hecht, *Optik*, 4th ed. München, Germany: Oldenbourg, 2005.
[8] S. Somiya, *Advanced Technical Ceramics*. Saint Louis, MO, USA: Elsevier Sci., 2014.
[9] Z. Chen et al., "3D printing of ceramics: A review," *J. Eur. Ceramic Soc.*, vol. 39, no. 4, pp. 661–687, 2019, doi: 10.1016/j.jeurceramsoc.2018.11.013.

[10] M. Schwentenwein, P. Schneider, and J. Homa, "Lithography-based ceramic manufacturing: A novel technique for additive manufacturing of high-performance ceramics," in *Proc. 13th Int. Ceramics Congr.*, 2014, pp. 60–64.
[11] J. Mollá, R. Moreno, and A. Ibarra, "Effect of MG doping on dielectric properties of alumina," *J. Appl. Phys.*, vol. 80, no. 2, pp. 1028–1032, 1996, doi: 10.1063/1.362836.
[12] J. Ornik, M. Sakaki, M. Koch, J. C. Balzer, and N. Benson, "3D printed Al 2 O 3 for terahertz technology," *IEEE Access*, vol. 9, pp. 5986–5993, 2021, doi: 10.1109/ACCESS.2020.3047514.
[13] A. Jimenez-Saez, M. Schusler, D. Pandel, N. Benson, and R. Jakoby, "3D printed 90 GHz frequency-coded chipless wireless RFID tag," in *Proc. IEEE MTT-S Int. Microw. Workshop Series Adv. Mater. Processes RF THz Appl. (IMWS-AMP)*, Bochum, Germany, Jul. 2019, pp. 4–6.
[14] A. Jimenez-Saez et al., "3D printed alumina for low-loss millimeter wave components," *IEEE Access*, vol. 7, pp. 40719–40724, 2019, doi: 10.1109/ACCESS.2019.2906034.
[15] T. Burmeister et al., "Chipless frequency-coded RFID tags integrating high-Q resonators and dielectric rod antennas," in *Proc. 15th Eur. Conf. Antennas Propag. (EuCAP)*, 2021, pp. 1–5.
[16] K.-D. Jenkel, B. Sievert, A. Rennings, M. Sakaki, D. Erni, and N. Benson, "Enhanced radar cross-section for W-band corner reflectors using ceramic additive manufacturing," in *Proc. IEEE 12th Int. Conf. RFID Technol. Appl. (RFID-TA)*, Cagliari, Italy, 2022, pp. 37–39.
[17] "LithaCon." Accessed: Mar. 2023. [Online]. Available: https://lithoz.com/de/materialien/lithacon-3y-210
[18] G. O. Mallory and J. B. Hajdu, *Electroless Plating: Fundamentals and Applications*. Orlando, FL, USA: Society, 1990.
[19] E. F. Knott, J. F. Shaeffer, and M. T. Tuley, *Radar Cross Section*, 2nd ed. Raleigh, NC, USA: SciTech, 2004.
[20] N. Reyes, F. Casado, V. Tapia, C. Jarufe, R. Finger, and L. Bronfman, "Complex dielectric permittivity of engineering and 3D-printing polymers at Q-band," *J. Infrared Millimeter Terahertz Waves*, vol. 39, no. 11, pp. 1140–1147, 2018, doi: 10.1007/s10762-018-0528-9.
[21] M. T. Sebastian, R. Ubic, and H. Jantunen, "Low-loss dielectric ceramic materials and their properties," *Int. Mater. Rev.*, vol. 60, no. 7, pp. 392–412, 2015, doi: 10.1179/1743280415Y.0000000007.
[22] Y. Oh et al., "Microwave dielectric properties of zirconia fabricated using NanoParticle Jetting^{TM}," *Additve Manuf.*, vol. 27, pp. 586–594, May 2019.
[23] T. Shimizu and Y. Kogami, "Frequency dependence measurements of complex permittivity for YSZ crystal plates by the cut-off circular waveguide method," in *Proc. Asia–Pacific Microw. Conf. (APMC)*, Yokohama, Japan, 2022, pp. 139–141.
[24] W. H. A. Fincham and M. H. Freeman, *Optics*, 8th ed. London, U.K.: Butterworths, 1974.

Kai-Daniel Jenkel was born in Moers, Germany, in 1992. He received the master's degree in nano process technology from the University of Duisburg-Essen, Germany, in 2018, where he is currently pursuing the Ph.D. degree with the Institute of Technology for Nanostructures. His current research interest includes the additive manufacturing of ceramics, especially for high frequency signal processing applications.

Benedikt Sievert (Member, IEEE) was born in Krefeld, Germany. He received the B.Sc. and M.Sc. degrees in electrical engineering/high-frequency systems from the University of Duisburg-Essen in 2017 and 2019, respectively, where he has been a member of the Laboratory of General and Theoretical Electrical Engineering since 2017. His research interests include mm-wave on-chip antennas, electromagnetic metamaterials, theoretical, and computational electromagnetics.

Andreas Rennings (Member, IEEE) received the Dipl.-Ing. and Dr.-Ing. degrees from the University of Duisburg-Essen in 2000 and 2008, respectively, where he studied electrical engineering. He carried out his diploma work during a stay with the University of California at Los Angeles, Los Angeles. From 2006 to 2008, he was with IMST GmbH, Kamp-Lintfort, Germany, where he worked as an RF engineer. Since then, he has been a Senior Scientist and a Principal Investigator with the Laboratory for General and Theoretical Electrical Engineering, University of Duisburg-Essen. His general research interests include all aspects of theoretical and applied electromagnetics, currently with a focus on medical applications and on-chip millimeter-wave/THz antennas. He received several awards, including a Student Paper Price at the 2005 IEEE Antennas and Propagation Society International Symposium and the VDE-Promotionspreis 2009 for the dissertation.

Masoud Sakaki received the Ph.D. degree in materials science and engineering in 2010. His main expertise is synthesis, characterization, and sintering of ceramic compounds via different routes. He was an Assistant Professor with Malayer University, Iran, from 2010 to 2014, and a Postdoctoral Researcher with Kochi University, Japan, from 2014 to 2019. He is currently a Postdoctoral Researcher with Duisburg-Essen University. His research is focused on the additive manufacturing of ceramics for THz applications.

Daniel Erni (Senior Member, IEEE) received the first Diploma degree in electrical engineering from the University of Applied Sciences in Rapperswil, Switzerland, in 1986, and the second Diploma degree in electrical engineering and the Ph.D. degree in laser physics from ETH Zurich in 1990 and 1996, respectively, where he has been working with the Laboratory for Electromagnetic Fields and Microwave Electronics since 1990. From 1995 to 2006, he was the Founder and the Head of the Communication Photonics Group, ETH Zurich. Since October 2006, he has been a Full Professor for General and Theoretical Electrical Engineering with the University of Duisburg-Essen, Germany. His current research interests include optical interconnects, nanophotonics, plasmonics, advanced solar cell concepts, optical and electromagnetic metamaterials, RF, mm-wave and THz engineering, biomedical engineering, bioelectromagnetics, marine electromagnetics, computational electromagnetics, multiscale and multiphysics modeling, numerical structural optimization, and science and technology studies. He is a co-founder of the spin-off company airCode on flexible printed RFID Technology. He is a Fellow of the Electromagnetics Academy, a member of the Center for Nanointegration Duisburg-Essen, as well as a member of the Swiss Physical Society, the German Physical Society (DPG), and OPTICA.

Niels Benson (Member, IEEE) received the Dipl. Ing. degree in electrical engineering from the University of Stuttgart in 2004, and the Dr. Ing. degree in materials science from Technische Universität Darmstadt in 2009. Since 2008, he has been a Senior Scientist for polymer vision on rollable active matrix displays. In 2010, he joined the University of Duisburg-Essen as a Research Group Leader on thin film photovoltaics and electronics. In 2018, he was appointed as a W1-Professor with the University of Duisburg-Essen on printable materials for signal processing systems. His current research interests include charge carrier transport in disordered semiconductor systems, passive chipless RFID systems, and additive manufactured ceramic components for sub-mm wave signal processing applications.